Check for updates

On the Nanomechanical and Viscoelastic Properties of Coatings Made of Recombinant Sea Star Adhesive Proteins

Mathilde Lefevre[1,2], Thi Quynh Tran[1], Thomas De Muijlder[1], Bede Pittenger[3], Patrick Flammang[4], Elise Hennebert[2] and Philippe Leclère[1]*

[1] Laboratory for Chemistry of Novel Materials, Research Institute for Materials, Department of Chemistry, University of Mons, Mons, Belgium, [2] Laboratory of Cell Biology, Research Institute for Biosciences, Department of Biology, University of Mons, Mons, Belgium, [3] Bruker Nano Surfaces, Atomic Force Microscopy Unit, Santa Barbara, CA, United States, [4] Biology of Marine Organisms and Biomimetics Unit, Research Institute for Biosciences, University of Mons, Mons, Belgium

To attach to surfaces in the sea, sea stars produce proteinaceous adhesive secretions. Sfp1 is a major constituent of this adhesive, where it is present in the form of four subunits (named Sfp1α to δ) displaying specific protein-, carbohydrate- and metal-binding domains. Recently, two recombinant proteins inspired from Sfp1 have been produced: one corresponding to the C-terminal part of Sfp1β and the other to the full-length Sfp1δ. Adsorption ability tests showed that both recombinant proteins were able to adsorb and to form coatings on different surfaces in artificial seawater as well as in Tris buffer supplemented with NaCl or $CaCl_2$. In this study, we used Atomic Force Microscopy (AFM) to characterize the nanomechanical properties of these coatings with an emphasis on functional characteristics such as adhesive properties and modulus of elasticity. We used AFM techniques which are the most appropriate to characterize the coating microstructure combined with the mapping of its nanomechanical properties.

Keywords: atomic force microscopy, adhesive proteins, nanomechanical AFM modes, viscoelastic properties, peakforce and quantitive imaging modes

INTRODUCTION

Nowadays, adhesion in wet environments is a crucial economic and medical concern (Almeida et al., 2020). In this context, glues inspired by adhesive secretions produced by marine organisms are increasingly being studied to replace currently available surgical adhesives and sealants which pose toxicity issues (e.g., cyanoacrylate or formaldehyde-based glues), or which cannot be used in areas continuously bathed with body fluids (e.g., fibrin) (Duarte et al., 2012; Annabi et al., 2014). The prerequisite of such applications is the complete molecular and functional characterization of these protein-based marine glues. To date, the best-characterized marine bioadhesive is that from the mussel and it has inspired most of the biomimetic adhesives currently available (see Waite, 2017 for review). DOPA (3,4-dihydroxy-L-phenylalanine), which is formed by the post-translational modification of tyrosine, is the key component of mussel glue, by displaying important interfacial adhesive and bulk cohesive roles (Heinzmann et al., 2016). A number of DOPA-based

inspired bioadhesives have therefore been developed, either in the form of recombinant preparations of mussel adhesive proteins or in the form of chemically synthesized polymers incorporating catechol groups (Kord Forooshani and Lee, 2017). The proteins constituting the adhesive secretions from other species like tubeworms, barnacles, echinoderms and flatworms are also being increasingly characterized and are considered as a source of inspiration for the development of new adhesives (e.g., Becker et al., 2012; Hennebert et al., 2014, Liang et al., 2019; Wunderer et al., 2019). For instance, Sfp1, a major sea star adhesive protein, presents a multimodular structure (i.e., four subunits, each comprising several protein-, carbohydrate- and metal-binding domains) which provides a relatively unexplored design paradigm for potential applications as adhesives and sealants (Hennebert et al., 2014).

The adhesion ability of biomimetic adhesives can be analyzed at the macro-scale by different methods such as tensile or lap-shear tests (e.g., Cha et al., 2009; Choi et al., 2012; Liang et al., 2015). Regarding the nano- and micro-scale, a powerful tool can be used, Atomic Force Microscopy (AFM). Different AFM modes widely described in literature have been developed to study biomolecules. For example, some mussel and barnacle recombinant proteins have been investigated using this technique to understand the topography of dried protein layers (e.g., Hwang et al., 2007; Liang et al., 2018). Chemical Force Microscopy (CFM) has also been used to characterize the adhesion of such proteins (Noy, 2006). This technique uses a modified cantilever presenting at its end a glass bead coated with the proteins of interest. For instance, the interaction between recombinant mussel proteins Mgfp-3A, Mgfp-5 and fp151 and clean glass surface was investigated by recording force-distance curves and showed that these proteins presented a higher adhesion force compared to the Cell-Tak® control (Hwang et al., 2004, 2005, 2007). The characterization of microscale adhesion of the recombinant barnacle protein Balcp19k was also performed using protein modified colloidal probes and AFM-based force spectroscopy (Liang et al., 2018).

Two recombinant sea star adhesive proteins, rSfp1 Beta C-term and rSfp1 Delta (Lefevre et al., 2020) are the focus of the present study. These two multimodular recombinant proteins adsorb on surfaces upon addition of Na^+ and/or Ca^{2+} ions. In artificial seawater (ASW), rSfp1 Beta C-term forms a meshwork (with component walls around 600 nm in height) made up of globular nanostructures about 160–200 nm in diameter, while in Tris buffer supplemented with 450 mM NaCl it forms a very dense homogeneous layer on the surface with smaller globular structures of 80–120 nm. As for rSfp1 Delta, it forms a very thin layer composed of very small globular nanostructures scattered homogeneously on the surface in Tris buffer supplemented with 150 mM $CaCl_2$ (Lefevre et al., 2020). These coatings were imaged in air using AFM in Tapping mode in our previous study (Lefevre et al., 2020). In the present study, we used AFM to image rSfp1 Beta C-term and rSfp1 Delta coatings and measure their mechanical properties at the nanoscale. All coatings were investigated using Peak Force Quantitative Nanomechanical Property Mapping (PF-QNM) both in air and in water. In addition, nanoscale dynamic mechanical analysis

(nDMA), a new technique based on AFM, was implemented to investigate the visco-elastic properties of rSfp1 Beta C-term coatings in fluid conditions. This technique is a new mode for quantitative viscoelastic analysis of heterogeneous polymer materials at the nanoscale. AFM-nDMA takes advantage of the exquisite force sensitivity, small contact radius, and nanoscale indentation depth of the AFM to provide dynamic mechanical analysis with 10 nm spatial resolution at rheologically relevant frequencies and variable temperature (Pittenger et al., 2019).

MATERIALS AND METHODS

Production of Recombinant Proteins rSfp1
The coding sequences for two parts of Sfp1 (rSfp1 Beta C-term and rSfp1 Delta) were inserted in a pET-28a (+) protein expression vector (Novagen) in frame with C-terminal 6 × His-tag coding sequence. The recombinant proteins were expressed in the *Escherichia Coli* C2566 strain (New England Biolabs) and purified using a HisTrap HP column (GE Healthcare) connected to an Akta Start system (GE Healthcare) under denaturing conditions as described in Lefevre et al. (2020). After a direct dialysis against 25 mM Tris to remove denaturing compounds, both proteins were stored at 4°C in 25 mM Tris buffer, pH 8 (Lefevre et al., 2020).

Preparation of Samples
The proteins were deposited on glass surfaces pre-cleaned with 5% HCl as described in Lefevre et al. (2020). Briefly, a 40 μl drop of a 0.2 mg/mL stock protein solution in 25 mM Tris buffer was deposited on glass and mixed with 40 μL of different buffers to generate the following conditions: (1) artificial sea water (ASW, 445 mM NaCl, 60 mM MgCl2, 10 mM KCl, 10 mM CaCl2, 2.4 mM NaHCO3, 10 mM Hepes, pH 8.0; Szulgit and Shadwick, 2000) in which rSfp1 Beta C-term forms a meshwork, (2) 25 mM Tris, 450 mM NaCl in which rSfp1 Beta C-term forms a homogeneous coating, and (3) 25 mM Tris, 150 mM $CaCl_2$ in which rSfp1 Delta (monomeric form) forms a homogeneous coating. These conditions were selected based on preliminary adsorption tests on glass coverslips (Lefevre et al., 2020). Bovine serum albumin (BSA) was used as a reference protein and the mix of rSfp1 Beta C-term and rSfp1 Delta was also characterized. In this case, a 20 μL drop of 0.2 mg/mL of each rSfp1 proteins in Tris buffer was mixed with 40 μL of buffers. The surfaces were incubated in a humid environment for 16 h at 25°C and then were washed thoroughly with deionized water for 2 h with shaking. For observations made in air, samples were prepared on microscope coverslips and air dried before measurements. For observations made in fluid, samples were prepared on microscope slides into a Gene Frame seal (ThermoFisher, **Supplementary Figure 1C**) and kept in a humid environment until the measurements.

Peak Force Quantitative Nanomechanical Property Mapping (PF-QNM)
Images were obtained by scanning the protein layer on glass surface in air under ambient conditions using AFM (Bruker, Icon Dimension + NanoScope V controller, Santa Barbara, CA, USA; Bruker NanoScope Software v9.7) operated using

the Peak Force QNM mode (Pittenger et al., 2010) at 25°C. To obtain topography profiles of samples, RTESPA 300-30 probes were used (Bruker AFM Probes, Camarillo, CA, USA; **Supplementary Figure 1A**). Theses silicon probes are pre-calibrated with rounded, well-defined tips, have a spring constant of ∼40 N/m and a tip radius of 30 nm (± 15%). The fluid experiments were performed in deionized water using a specific pre-calibrated probe, the so-called PFQNM-LC-A-CAL (Bruker AFM Probes, Camarillo, CA, USA), particularly suited for biological samples (**Supplementary Figure 1C**). This short paddle-shaped cantilever has a pre-calibrated spring of ∼0.1 N/m, a resonance frequency of ∼45 kHz and a 70 nm radius (**Supplementary Figure 1B**). This tip is particularly useful for imaging soft materials like cells (e.g., Berquand et al., 2019, Efremov et al., 2020). The deflection sensitivity has also been calibrated using ramping on sapphire substrate and was ∼38 nm/V. The peak force amplitude was 300 nm, the scan rate was 0.1 Hz at a peak force frequency of 0.5 kHz. All the captured images were recorded with a resolution of 256 × 256 data points. For each pixel of the image, a force curve was also recorded. Adhesion was measured during pull-off force-distance curve and corresponds to the minimum of the curve. The other quantitative mechanical properties (i.e., rigidity modulus, deformation, …) were obtained using Bruker software applying the Johnson-Kendall-Roberts (JKR) model (Johnson et al., 1971; NanoScope Analysis v2.0). This model is a contact mechanics model which adapted Hertz theory by adding adhesion forces. JKR is known to be be the most appropriate for soft and sticky materials. In that case, the adhesion effect on the contact region shape cannot be neglected. So, unlike the DMT model, it takes into account only the adhesion forces that come inside the contact region (Johnson and Greenwood, 1997).

Nanoscale Dynamic Mechanical Analysis (nDMA)

AFM images were also obtained for the coating formed by rSfp1 Beta C-term in artificial seawater on glass surface, rinsed, and scanned in deionized water using AFM operated using the nDMA mode, and fast force volume measurement. For these fluid measurement, a PFQNM-LC-A-CAL probe was also used. The ramp size was 300 nm and the ramp rate was 5 Hz. The modulate amplitude was 1 mV and the hold time 500 ms. The drive frequency used was 80 Hz and the same drive frequency was applied during the calibration on glass experiment. The calibration allows compensation for the phase shift between Z and deflection (φ – ψ) that occurs in both air and liquid. It is expected that there is an additional drag force on the cantilever in liquid that will influence the measurement slightly. For this work, we do not attempt to compensate for this, but instead assume that the drag force at 80 Hz is small compared to the oscillatory force from the cantilever spring. This technique is able to provide the storage modulus (E'), the loss modulus (E"), and the ratio E"/E' corresponding to loss tangent or tan δ (Pittenger et al., 2019). Because the measurement takes place during the "hold segment" of the force-distance curve (i.e; when the tip is located and stay at the vertical of one pixel), these properties are largely decoupled

from the tip-sample adhesion—an important consideration when studying adhesives (Pittenger et al., 2019). The model of AFM-nDMA are described in Pittenger et al. (2019). This mode operates through application of sinusoidal motion to a Z piezo and measurement of resulting low-amplitude oscillating motion of the tip in contact with the sample. Viscoelastic properties are determined through the resulting amplitude and phase shift of the cantilever oscillation. The Z piezo motion as a function of time is described by

$$z(t) = Z_1 \sin(\omega t + \psi)$$

Where Z_1 is the amplitude of Z motion, ω is the measurement frequency, and ψ is its phase. Likewise, the cantilever deflection as a function of time is described by

$$d(t) = D_1 \sin(\omega t + \varphi)$$

Where D_1 is the cantilever deflection amplitude, and φ is the deflection phase. The amplitude ratio (D_1/Z_1) and phase shift ($\varphi - \psi$) are extracted to yield the complex "dynamic stiffness," S*:

$$S^* = S' + iS'' = \frac{force}{deformation} = \frac{K_c D_1 e^{i\varphi}}{(Z_1 e^{i\psi} - D_1 e^{i\varphi})}$$

Where K_c is the cantilever spring constant. The real and imaginary parts of S∗ can then be separated into storage stiffness (S') and loss stiffness (S"), respectively, while the loss tangent (also known as tan δ) is simply the ratio of the two:

$$S' = \frac{K_c D_1}{Z_1} \frac{\cos(\varphi - \psi) - D_1/Z_1}{[\cos(\varphi - \psi) - D_1/Z_1]^2 + [\sin(\varphi - \psi)]^2}$$

$$S'' = \frac{K_c D_1}{Z_1} \frac{\sin(\varphi - \psi)}{[\cos(\varphi - \psi) - D_1/Z_1]^2 + [\sin(\varphi - \psi)]^2}$$

$$\tan \delta = \frac{S'}{S''} = \frac{\sin(\varphi - \psi)}{\cos(\varphi - \psi) - (D_1/Z_1)}$$

Unsupervised Clustering Data

To analyze AFM data, a multi-dimensional data analysis based on KMeans (MacQueen, 1967), a unsupervised clustering algorithm, was performed. KMeans is aimed to sort pixels in k clusters by using the measured properties of the sample. These properties are normalized by min-max normalization to give them an equal weight for the clustering. If the sample can be described in terms of different populations, each one will correspond to a different cluster. After the clustering, populations can be characterized separately by histograms, boxplots, and so on. It is also possible to map the different clusters to highlights the presence of nanostructures in the sample.

The properties used for the clustering were chosen thanks to a Spearman correlation test. When two properties are strongly correlated (i.e., |rs| > 0.7), it is often better to only use one of them to avoid the use of redundant information during the clustering.

RESULTS

Topography of rSfp1 Coatings

First, AFM was used to provide topographic images and roughness measurements for each Peak Force Quantitative

Nanomechanical Property Mapping (PF-QNM) image of the rSfp1 coatings both in air and underwater (**Table 1**). As expected, in air, the roughness of Sfp1 Beta C-term coatings were higher than those of rSfp1 Delta (Lefevre et al., 2020), while the roughness of the coatings made up by the mix of the two recombinant proteins was intermediate. Excepted for rSfp1 Delta, the roughness of all the coatings was lower in deionized water than in air. This could be explained by the fact that the globular nanostructures composing these coatings swell in deionized water, thereby limiting the roughness at the nanometer scale (**Supplementary Figure 2**).

In air, the coating made up of rSfp1 Beta C-term ASW was composed of nanoglobular structures of 80–200 nm while coatings prepared in Tris buffer supplemented with 450 mM NaCl (rSfp1 Beta C-term 450 mM NaCl) possessed smaller globular structures (90–150 nm) with some bigger at 400 nm (**Figures 1A,B**). When observed in deionized water, rSfp1 Beta C-term ASW f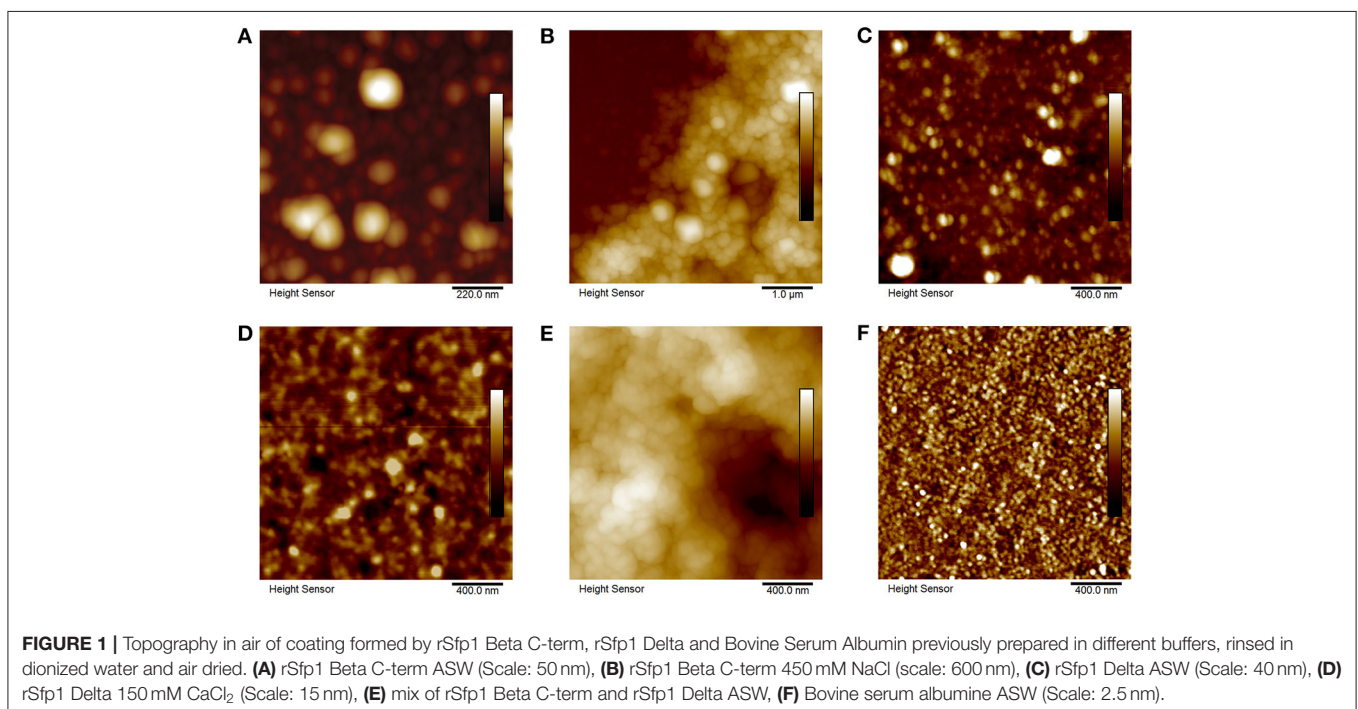ormed a thin layer (few hundreds of nm) with smaller nanostructures then in air (around 30 to 70 nm, **Figures 2A,D**, **Supplementary Figure 2**) while the topography of rSfp1 Beta C-term 450 mM NaCl did not change much, with a large number of globular structures at 80–120 nm, the biggest ones being around 250 nm (**Figure 3A**). Regarding rSfp1 Delta prepared in ASW (rSp1 Delta ASW), in air, it formed a homogenous layer with aggregates of 60–100 nm, while in deionized water, globular nanostrutures were around 75–130 nm with bigger ones of 180 nm (**Figures 1C, 3D**). When rSfp1 Delta was prepared in Tris buffer supplemented with 150 mM CaCl$_2$ (rSfp1 Delta 150 mM CaCl$_2$), the proteins formed small nanoglobular structures of 50–90 nm in air and of 80–140 nm in deionized water (**Figures 1D, 3G**). Finally, for the mix of both recombinant proteins prepared in ASW (mix of rSfp1 Beta C-term and rSfp1 Delta ASW), globular structures around 80–130 nm were observed in air (**Figure 1E**) which were sligthy smaller than in rSfp1 Beta C-term ASW and rSfp1 Delta ASW coatings. In deionized water, the mix of rSfp1 Beta C-term and rSfp1 Delta ASW showed a flatter layer compared to air, with globular structures of 100–140 nm (**Figure 3J**). As control, Bovine Serum Albumine prepared in ASW (BSA ASW) was also analyzed using Peak Force QNM mode and showed a very smooth layer (with a roughness of 2.5 nm) in air and in dionized water without any distinguishable structure (**Figures 1F, 3M**).
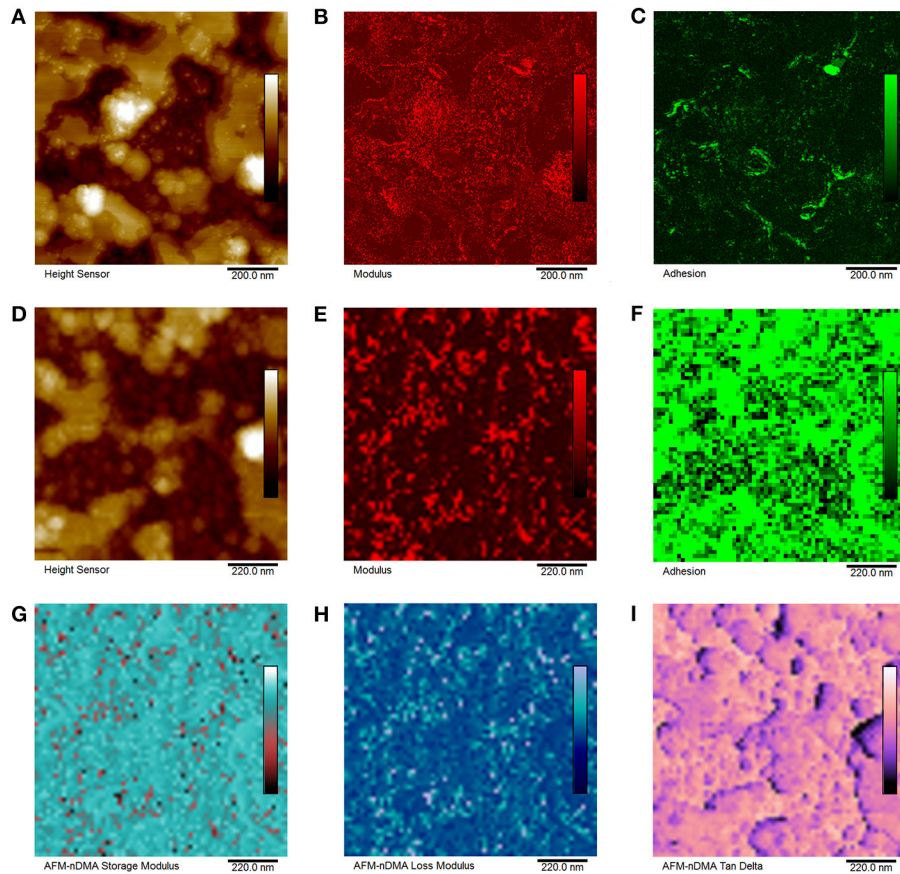
Nanomechanical Properties of Proteins Layers

The nanomechanical properties of the rSfp1 coatings were investigated using PF-QNM and nanoscale Dynamic Mechanical Analysis (nDMA) in deionized water (**Table 2**). For these experiments, BSA was used as a reference protein as its molecular

TABLE 1 | Roughness (Rq) calculated from height images obtained using PF-QNM measurement of rSfp1 coatings.

	Rq (nm)	
	Air	Deionized water
rSfp1 Beta C-term ASW	129	8.48
rSfp1 Beta C-term 450 mM NaCl	66.9	23.2
rSfp1 Delta ASW	3.11	1.8
rSfp1 Delta 150 mM CaCl$_2$	1.71	8.84
Mix of rSfp1 Beta C-term and rSfp1 Delta ASW	31.2	16.7

FIGURE 1 | Topography in air of coating formed by rSfp1 Beta C-term, rSfp1 Delta and Bovine Serum Albumin previously prepared in different buffers, rinsed in dionized water and air dried. **(A)** rSfp1 Beta C-term ASW (Scale: 50 nm), **(B)** rSfp1 Beta C-term 450 mM NaCl (scale: 600 nm), **(C)** rSfp1 Delta ASW (Scale: 40 nm), **(D)** rSfp1 Delta 150 mM CaCl$_2$ (Scale: 15 nm), **(E)** mix of rSfp1 Beta C-term and rSfp1 Delta ASW, **(F)** Bovine serum albumine ASW (Scale: 2.5 nm).

FIGURE 2 | Nanomechanical mapping of rSfp1 Beta C-term coating prepared in artificial sea water and observed in deionized water using **(A,C)** Peak Force QNM mode, **(D–I)** nDMA mode in fluid. **(A)** Height, scale: 50 nm, **(B)** Modulus, scale: 10 MPa, **(C)** Adhesion, scale: 500 pN, **(D)** Height in nDMA mode, scale: 50 nm, **(E)** Modulus, scale: 10 MPa, **(F)** Adhesion, scale: 500 pN, **(G)** Storage modulus, scale: 17.5 MPa, **(H)** Loss modulus, scale: 15 MPa, and **(I)** Tan Delta, scale: 0.400.

weight and isoelectric point are close to those of rSfp1s. Random spots were analyzed on areas without large structures but close to these.

The measured moduli were 300 MPa for rSfp1 Beta C-term ASW for both modes used, and 500 MPa for rSfp1 Beta C-term NaCl (**Figures 2B,E**, **3B**). These values are close to those expected for biological samples (Lakes, 2009). The adhesion was comprised between 90 and 300 pN for rSfp1 Beta C-term ASW and was 200 pN for rSfp1 Beta C-term 450 mM NaCl (**Figures 2C,F**, **3C**). The coating formed in ASW is homogeneous at nanomechanical level and no cluster was observable. The visco-elastic properties of rSfp1 Beta C-term ASW were also analyzed. The storage modulus and loss modulus were 40 and 20 MPa, respectively, and the tan δ was 0.2 (**Figures 2G–I**).

rSfp1 Delta ASW and rSfp1 Delta 150 mM CaCl$_2$ presented a modulus of 5 MPa and 500 kPa, respectively (**Figures 3E,H**). Regarding the adhesion, values were also higher with 150 pN for rSfp1 Delta ASW and lower with 80 pN for rSfp1 Delta 150 mM CaCl$_2$ (**Figures 3F,I**).

The coating made up of the two recombinant proteins and prepared in ASW presented a homogeneous mapping of the nanomechanical properties, with an adhesion force (70 pN) in the same range as that of rSfp1 Beta C-term ASW and rSfp1 Delta ASW. The modulus (10 MPa), on the other hand, was similar to that of rSfp1 Delta ASW but much lower than that of rSfp1 Beta C-term ASW (**Figures 3K,L**).

As control, BSA ASW was also analyzed using Peak Force QNM mode and showed an adhesion of 100 pN and a modulus of 5 MPa (**Figures 3N,O**).

DISCUSSION

Adhesion in fluid and saline environments is an interesting and promising field as much for industry as for the medical and dental fields. Nowadays, biomimetic strategies are often employed to develop new adhesive materials (Almeida et al., 2020). Up to now, most studies have investigated the permanent adhesive mechanism of mussels and barnacles, but the temporary adhesion of sea stars has gained interest in recent years (Hennebert et al., 2014; Lengerer et al., 2019; Lefevre et al., 2020). In the study of biological adhesives, AFM was already used to determine the adhesion ability of natural glues but also of recombinant adhesive proteins. To the best of our knowledge,
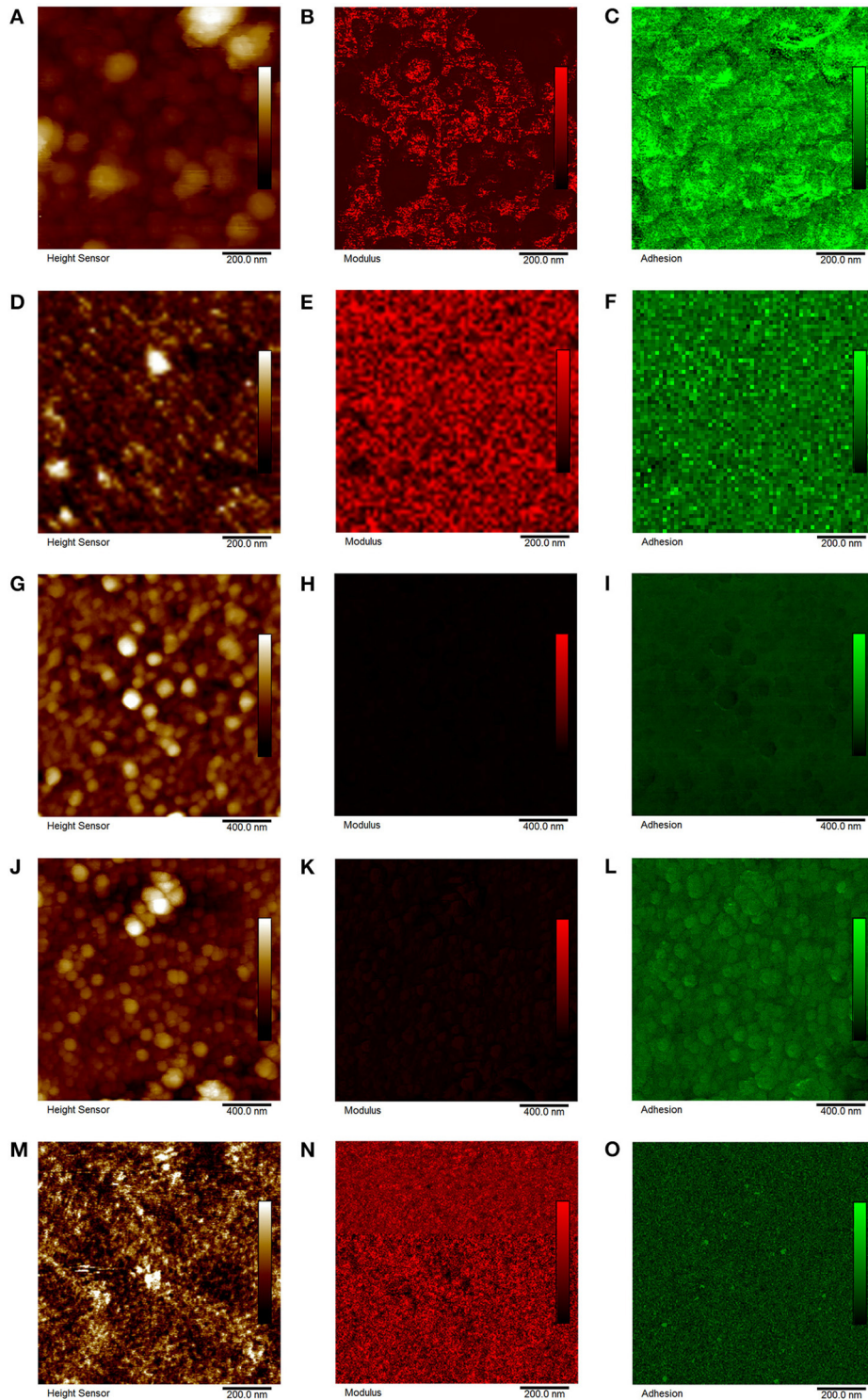
FIGURE 3 | Nanomechanical mapping of **(A–C)** rSfp1 Beta C-term 450 mM NaCl, **(D–F)** rSfp1 Delta ASW, **(G–I)** rSfp1 Delta 150 mM CaCl$_2$, **(J–L)** mix of rSfp1 Beta C-term and rSfp1 Delta ASW, **(N–P)** Bovine serum albumin ASW using Peak Force QNM mode in fluid (observations made in deionized water). **(A)** Height, scale: 200 nm, **(B)** Modulus, scale: 10 MPa, **(C)** Adhesion, scale: 500 pN, **(D)** Height, scale: 15 nm, **(E)** Modulus, scale: 10 MPa, **(F)** Adhesion, scale: 500 pN, **(G)** Height, scale: 70 nm, **(H)** Modulus, scale: 10 MPa, **(I)** Adhesion, scale: 500 pN, **(J)** Height, scale: 115 nm, **(K)** Modulus, scale: 10 MPa, **(L)** Adhesion, scale: 500 pN, **(M)** Height, scale: 2.5 nm, **(N)** Modulus, scale: 10 MPa, and **(O)** Adhesion, scale: 500 pN.

TABLE 2 | Peak Force Quantitative Nanomechanical Property Mapping (PF-QNM) and nanoscale dynamic mechanical analysis (nDMA) of rSfp1 coatings.

	PF-QNM		nDMA				
	Adhesion (pN)	JKR modulus (MPa)	Adhesion (pN)	JKR modulus (MPa)	Storage modulus (MPa)	Loss modulus (MPa)	Tan δ (mU)
rSfp1 Beta C-term ASW	90 ± 20	300 ± 50	300 ± 100	300 ± 45	40 ± 10	20 ± 7.5	500 ± 50
rSfp1 Beta C-term 450 mM NaCl	200 ± 75	500 ± 100	–	–	–	–	–
rSfp1 Delta ASW	150 ± 50	5 ± 1	–	–	–	–	–
rSfp1 Delta 150 mM CaCl₂	80 ± 20	0.5 ± 0.05	–	–	–	–	–
Mix of rSfp1 Beta C-term and rSfp1 Delta ASW	70 ± 20	10 ± 2	–	–	–	–	–
BSA ASW	100 ± 25	5 ± 1	–	–	–	–	–

the combination of PF-QNM and AFM-nDMA modes has never been applied before to investigate the nanomechanical properties of coatings composed of recombinant adhesives proteins.

In this study, coatings formed by recombinant proteins based on the sequence of the adhesive protein Sfp1 from the sea star *Asterias rubens* were investigated. The nanomechanical properties of films made up of rSfp1 proteins were previously unknown. Two proteins (rSfp1 Beta C-term and rSfp1 delta) were used separately or in combination, and coatings were made in different solutions (ASW, NaCl, and CaCl₂). Using PF-QNM, the adhesion of the coatings measured in deionized water ranged from 70 to 200 pN and their modulus from 0.5 to 300 MPa. Coatings consisting of rSfp1 Beta C-term were stiffer and more adhesive than those made up of rSfp1 Delta. When the two proteins were mixed, the properties of the resulting coatings were closer to those of films made of rSfp1 Delta alone. For the control protein, BSA, these values were 100 pN and 5 MPa, respectively. The moduli of some protein-based materials are know, such as elastin in which the Young's modulus is about 0.6 MPa (Fung and Sobin, 1981), or collagen fibers for which it is 1 GPa (Hiltner et al., 1985). rSfp1 proteins are certainly on the soft side of this range. Their adhesivity, on the other hand, is in the same order of magnitude than that of the negative control BSA. These results could be explained by the cohesive function of Sfp1 in the native adhesive. Indeed, Sfp1 is located in the meshwork of the adhesive footprint and not in direct contact with the surface (Hennebert et al., 2014).

The effect of hydration of human serum abumin (HSA) proteins layer have been studied in Lubarsky et al. (2007). They showed that the thickness and layer density of HSA layer increased when water is adsorbed but also that the viscosity and the modulus were higher for the dry layer. These values were similar to those obtained for rSfp1, with a range of 500 kPa to 2.5 GPa in dry conditions.

To quantify the adhesion ability of mussel recombinant proteins, Hwang et al. used another method. Indeed, the analysis of the adhesion force of recombinant Mgfp-5, Mgfp-3A and a recombinant hybrid mussel bioadhesive fp-151 was performed via force-distance curves using a modified AFM cantilever (Hwang et al., 2004, 2005, 2007). A glass sphere with a radius of 20 μm was fixed to the cantilever tip with epoxy resin and

this modified tip was placed in contact with sample solutions for a determined time. The force-distance curve was obtained by separation of the coated cantilever from the glass surface. BSA was also used as a negative control, and commercial Cell-Tak was used as a positive control. These AFM measurements showed that the average adhesion force of tyrosine modified Mgfp-3A (~230 nN) was much higher that that of modified BSA (~30 nN), similar to that of modified Cell-Tak (~240 nN), and lower than that of modified recombinant Mgfp-5 (~550 nN) and hybrid fp-151 (~500 nN). All of these values are significantly higher than those obtained in the present study for recombinant Sfp1 proteins. This difference could be explained by the much larger contact area used in the case of recombinant mussel proteins. The advantage of using PeakForce QNM, in our case, is the ability to measure variations in adhesion and elasticity on a same protein coating at a smaller scale based on controled contact geometry. Indeed, both PeakForce QNM and the more general "force-volume" imaging involve acquiring topographic images and nanomechanical mapping simultaneously, allowing identification of elastic properties and pull-off force values with specific regions of a sample (Grierson et al., 2005).

For a soft protein coating, it is also important to measure visco-elastic properties. The visco-elastic behavior of reversible adhesives was particulary studied for the fracture or peeling of soft materials to understand how these soft materials and their visco-elastic properties affected their breakage and detachment from solid surfaces (Creton and Ciccotti, 2016; Perrin et al., 2019). In addition to the mapping of nanomechical properties by PF-QNM, the analysis of one sample by fast force volume in AFM-nDMA mode allowed to measure the visco-elastic properties determined by storage modulus, loss modulus and tan δ. The values of adhesion and JKR modulus obtained for the rSfp1 Beta C-term coating prepared in ASW were similar to those obtained with PF-QNM though slightly higher. The value measured for tan δ was 0.2, corresponding to a soft and visco-elastic material. As described in Lakes (2009), tan δ values between 10^{-1} and 10^{0} correspond to rubber, foam rubber, gels but also polymers.

In conclusion, we were able to successfully characterize the mechanical properties as well as the visco-elastic properties of soft coatings formed by recombinant adhesives proteins from marine organisms. The combination of PF-QNM and

AFM-nDMA techniques should be used for other marine adhesive systems or polymers to understand the impact of visco-elasticity in the adhesive abilities of bio-inspired materials. Futhermore, in next step, the analysis of visco-elastic properties should be performed, for each recombinant proteins, at different drive frequencies. Indeed, the elastic properties are expected to depend on frequency and temperature (Pittenger et al., 2019). The measurement of these properties at lower frequency could improve our knowledge about the mechanical properties of rSfp1.

DATA AVAILABILITY STATEMENT

The raw data supporting the conclusions of this article will be made available by the authors, without undue reservation.

AUTHOR CONTRIBUTIONS

ML, EH, PF, and PL designed the study and wrote the paper. ML and TQT performed the experiments. TD designed the Python code for the unsupervised clustering analysis. BP provided advice regarding AFM nanomechanics and suggestions regarding strategy for analysis. All authors revised and approved the final manuscript.

FUNDING

SUPPLEMENTARY MATERIAL

The Supplementary Material for this article can be found online at: https://www.frontiersin.org/articles/10.3389/fmech.2021.667491/full#supplementary-material

REFERENCES

Almeida, M., Reis, R. L., and Silva, T. H. (2020). Marine invertebrates are a source of bioadhesives with biomimetic interest. *Mater. Sci. Eng. C. Mater. Biol. Appl.* 108:110467. doi: 10.1016/j.msec.2019.110467

Annabi, N., Tamayol, A., Shin, S. R., Ghaemmaghami, A. M., Peppas, N. A., and Khademhosseini, A. (2014). Surgical materials: current challenges and nano-enabled solutions. *Nano Today* 9, 574–589. doi: 10.1016/j.nantod.2014.09.006

Becker, P. T., Lambert, A., Lejeune, A., Lanterbecq, D., and Flammang, P. (2012). Identification, characterization, and expression levels of putative adhesive proteins from the tube-dwelling polychaete *Sabellaria alveolata*. *Biol. Bull.* 223, 217–225. doi: 10.1086/BBLv223n2p217

Berquand, A., Meunier, M., Thevenard-Devy, J., Ivaldi, C., Campion, O., Dedieu, S., et al. (2019). A gentle approach to investigate the influence of LRP-1 silencing on the migratory behavior of breast cancer cells by atomic force microscopy and dynamic cell studies. *Nanomed. Nanotechnol. Biol. Med.* 18, 359–370.

Cha, H. J., Hwang, D. S., Lim, S., White, J. D., Matos-Perez, C. R., and Wilker, J. J. (2009). Bulk adhesive strength of recombinant hybrid mussel adhesive protein. *Biofouling* 25, 99–107. doi: 10.1080/08927010802563108

Choi, Y. S., Yang, Y. J., Yang, B., and Cha, H. J. (2012). *In vivo* modification of tyrosine residues in recombinant mussel adhesive protein by tyrosinase co-expression in Escherichia coli. *Microb. Cell Fact* 11:139. doi: 10.1186/1475-2859-11-139

Creton, C., and Ciccotti, M. (2016). Fracture and adhesion of soft materials: a review. *Rep. Prog. Phys.* 79:046601. doi: 10.1088/0034-4885/79/4/046601

Duarte, A. P., Coelho, J. F., Bordado, J. C., Cidade, M. T., and Gil, M. H. (2012). Surgical adhesives: systematic review of the main types and development forecast. *Prog. Polym. Sci.* 37, 1031–1050. doi: 10.1016/j.progpolymsci.2011.12.003

Efremov, Y. M., Kotova, S. L., Akovantseva, A. A., and Timashev, P. S. (2020). Nanomechanical properties of enucleated cells: contribution of the nucleus to the passive cell mechanics. *J. Nanobiotechnol.* 18:134. doi: 10.1186/s12951-020-00696-1

Fung, Y. C., and Sobin, S. S. (1981). The retained elasticity of elastin under fixation agents. *J. Biomech. Eng.* 103, 121–122. doi: 10.1115/1.3138255

Grierson, D. S., Flater, E. E., and Carpick, R. W. (2005). Accounting for the JKR–DMT transition in adhesion and friction measurements with atomic-force microscopy. *J. Adhes. Sci. Technol.* 19, 291–311. doi: 10.1163/1568561054352685

Heinzmann, C., Weder, C., and de Espinosa, L. M. (2016). Supramolecular polymer adhesives: advanced materials inspired by nature. *Chem. Soc. Rev.* 45, 342–358. doi: 10.1039/C5CS00477B

Hennebert, E., Wattiez, R., Demeuldre, M., Ladurner, P., Hwang, D. S., Waite, J. H., et al. (2014). Sea star tenacity mediated by a protein that fragments, then aggregates. *Proc. Natl. Acad. Sci. U.S.A.* 111, 6317–6322. doi: 10.1073/pnas.1400089111

Hiltner, A., Cassidy, J. J., and Baer, E. (1985). Mechanical properties of biological polymers. *Annu. Rev. Mater. Sci.* 15, 455–482. doi: 10.1146/annurev.ms.15.080185.002323

Hwang, D. S., Gim, Y., and Cha, H. J. (2005). Expression of functional recombinant mussel adhesive protein type 3A in *Escherichia coli*. *Biotechnol Progress* 21, 965–970. doi: 10.1021/bp050014e

Hwang, D. S., Gim, Y., Yoo, H. J., and Cha, H. J. (2007). Practical recombinant hybrid mussel bioadhesive fp-151. *Biomaterials* 28, 3560–3568. doi: 10.1016/j.biomaterials.2007.04.039

Hwang, D. S., Yoo, H. J., Jun, J. H., Moon, W. K., and Cha, H. J. (2004). Expression of functional recombinant mussel adhesive protein Mgfp-5 in *Escherichia coli*. *Appl. Environ. Microbiol.* 70, 3352–3359. doi: 10.1128/AEM.70.6.3352-3359.2004

Johnson, K. L., and Greenwood, J. A. (1997). An adhesion map for the contact of elastic spheres. *J. Colloid. Interface Sci.* 192, 326–333. doi: 10.1006/jcis.1997.4984

Johnson, K. L., Kendall, K., Roberts, A. D., and Tabor, D. (1971). Surface energy and the contact of elastic solids. *Proc. R. Soc. Lond. A. Math. Phys. Sci.* 324, 301–313. doi: 10.1098/rspa.1971.0141

Kord Forooshani, P., and Lee, B. P. (2017). Recent approaches in designing bioadhesive materials inspired by mussel adhesive protein. *J. Polym. Sci. Part A: Polym. Chem.* 55, 9–33. doi: 10.1002/pola.28368

Lakes, R. (2009). *Viscoelastic Materials*. Cambridge: Cambridge University Press.

Lefevre, M., Flammang, P., Aranko, A. S., Linder, M. B., Scheibel, T., Humenik, M., et al. (2020). Sea star-inspired recombinant adhesive proteins self-assemble and adsorb on surfaces in aqueous environments to form cytocompatible coatings. *Acta Biomater.* 112, 62–74. doi: 10.1016/j.actbio.2020.05.036

Lengerer, B., Algrain, M., Lefevre, M., Delroisse, J., Hennebert, E., and Flammang, P. (2019). Interspecies comparison of sea star adhesive proteins. *Phil. Trans. R. Soc. B.* 374:20190195. doi: 10.1098/rstb.2019.0195

Liang, C., Li, Y., Liu, Z., Wu, W., and Hu, B. (2015). Protein aggregation formed by recombinant cp19k homologue of balanus albicostatus combined with

an 18 kDa N-terminus encoded by pET-32a(+) plasmid having adhesion strength comparable to several commercial glues. *PLoS ONE* 10:e0136493. doi: 10.1371/journal.pone.0136493

Liang, C., Strickland, J., Ye, Z., Wu, W., Hu, B., and Rittschof, D. (2019). Biochemistry of barnacle adhesion: an updated review. *Front. Mar. Sci.* 6:565. doi: 10.3389/fmars.2019.00565

Liang, C., Ye, Z., Xue, B., Zeng, L., Wu, W., Zhong, C., et al. (2018). Self-assembled nanofibers for strong underwater adhesion: the trick of barnacles. *ACS Appl. Mater. Interfaces* 10, 25017–25025. doi: 10.1021/acsami.8b04752

Lubarsky, G. V., Davidson, M. R., and Bradley, R. H. (2007). Hydration–dehydration of adsorbed protein films studied by AFM and QCM-D. *Biosens Bioelectron* 22, 1275–1281. doi: 10.1016/j.bios.2006.05.024

MacQueen, J. (1967). "Some methods for classification and analysis of multivariate observations." in *Fifth Berkeley Symposium on Mathematical Statistics and Probability* (Berkeley, CA: University of California Press), 281–297.

Noy, A. (2006). Chemical force microscopy of chemical and biological interactions. *Surf. Interface Anal.* 38, 1429–1441. doi: 10.1002/sia.2374

Perrin, H., Eddi, A., Karpitschka, S., Snoeijer, J. H., and Andreotti, B. (2019). Peeling an elastic film from a soft viscoelastic adhesive: experiments and scaling laws. *Soft Matter.* 15, 770–778. doi: 10.1039/C8SM01946K

Pittenger, B., Erina, N., and Su, C. (2010). *Quantitative Mechanical Property Mapping at the Nanoscale with PeakForce QNM*. Santa Barbara, CA: Bruker Application Note.

Pittenger, B., Osechinskiy, S., Yablon, D., and Mueller, T. (2019). Nanoscale DMA with the atomic force microscope: a new method for measuring viscoelastic properties of nanostructured polymer materials. *JOM* 71, 3390–3398. doi: 10.1007/s11837-019-03698-z

Szulgit, G. K., and Shadwick, R. E. (2000). Dynamic mechanical characterization of a mutable collagenous tissue: response of sea cucumber dermis to cell lysis and dermal extracts. *J. Exp. Biol.* 203:1539.

Waite, J. H. (2017). Mussel adhesion – essential footwork. *J. Exp. Biol.* 220, 517–530. doi: 10.1242/jeb.134056

Wunderer, J., Lengerer, B., Pjeta, R., Bertemes, P., Kremser, L., Lindner, H., et al. (2019). A mechanism for temporary bioadhesion. *Proc. Natl. Acad. Sci. U.S.A.* 116, 4297–4306. doi: 10.1073/pnas.1814230116